arXiv:1603.04157v1 [physics.atom-ph] 14 Mar 2016

Ab-initio electron scattering cross-sections and transport in liquid xenon

G. J. Boyle,[1] R. P. McEachran,[2] D. G. Cocks,[1] M. J. Brunger,[3,4] S. J. Buckman,[2,4] S. Dujko,[5] and R. D. White[1]

[1]*College of Science, Technology & Engineering, James Cook University, Townsville 4810, Australia*

[2]*Plasma and Positron Research Laboratory, Research School of Physical Sciences and Engineering, Australian National University, Canberra, ACT 0200, Australia*

[3]*School of Chemical and Physical Sciences, Flinders University, Adelaide, SA 5001, Australia*

[4]*Institute of Mathematical Sciences, University of Malaya, 50603 Kuala Lumpur, Malaysia*

[5]*Institute of Physics, University of Belgrade, Pregrevica 118, 11080 Belgrade, Serbia*

Abstract

Ab-initio fully differential cross-sections for electrons scattering in liquid xenon are developed from a solution of the Dirac-Fock scattering equations, using a recently developed framework [1] which considers multipole polarizabilities, a non-local treatment of exchange, and screening and coherent scattering effects. A multi-term solution of Boltzmann's equation accounting for the full anisotropic nature of the differential cross-section is used to calculate transport properties of excess electrons in liquid xenon. The results were found to agree to within 25% of the measured mobilities and characteristic energies over the reduced field range of 10^{-4}–1 Td. The accuracies are comparable to those achieved in the gas phase. A simple model, informed by highly accurate gas-phase cross-sections, is presented to improve the liquid cross-sections, which was found to enhance the accuracy of the transport coefficient calculations.

I. INTRODUCTION

An understanding of the behavior of free electrons in liquids and dense systems is of interest to both fundamental physics research and to technological applications [1]. In particular, liquid-phase noble gases are used in high-energy particle detectors and at present several LAr (liquid argon) and LXe (liquid xenon) TPCs (time projection chambers) have been built for dark matter searches [2–6], neutrino detection [3, 6–8], and have also been used in high-energy beam-line experiments [6, 9]. Optimizing the performance of these liquid TPC particle detectors requires an accurate understanding of electron drift and diffusion in noble liquids subject to electric fields. In a previous paper, Boyle et al. [1], we investigated the elastic scattering of electrons from gas-phase and liquid-phase argon. In this paper, we extend the previous discussion to consider elastic scattering of electrons in gas-phase and liquid-phase xenon, using the same techniques previously outlined [1].

The study of excess electrons in dense gases and liquids involves many effects that are not significant in dilute gaseous systems. When the de Broglie wavelength of the electrons (near thermal energies) is comparable to the interatomic spacing of the medium, scattering occurs off multiple scattering centres simultaneously, rather than through binary scattering. Furthermore, these scattering centres are highly correlated in space and time. Historically, transport simulations neglected these correlations and simply scaled calculations in the dilute gas phase to higher densities. It has been shown [1] that this simplistic approach cannot explain the non-linearities seen in the experiments . As we have described in Boyle et al. [1], there are other theoretical approaches to exploring the effect of liquid correlations on the transport of light particles [10–15], however these either require empirical inputs, are applicable only close to equilibrium, or have heuristically combined the liquid effects identified above to obtain an effective cross-section.

As also discussed in Boyle et al. [1], we employ the *ab initio* procedure of Cohen and Lekner [16] using updated scattering theory to address transport in dense systems under a kinetic theory framework. Atrazhev et al. [17] have used a similar procedure based on a simplification of the Cohen and Lekner theory where they argued that, for small energies, the effective cross-section becomes dependent on the density only and they obtained good agreement with experiment. However, the distance at which to enforce this new behaviour of the effective cross-section remains a free parameter in the theory and this constant effective

cross-section must be found empirically. By performing a detailed analysis of the partial phase shifts, Atrazhev and co-workers [18] were able to isolate the important properties of the potential which are required for accurate determination of the transport properties. Our calculations instead avoid these difficulties by using accurate forms for the electron-atom interaction. The transport theory employed in this manuscript also represents an improvement over previous calculations as we use a full multi-term treatment of the velocity distribution function [14, 19] which utilizes all the available anisotropic details of the scattering cross-sections. It is well known that the often-used two-term approximation for transport calculations can be in serious error [20], and we compare our solutions for transport in the xenon system using two-term and multi-term treatments.

In the following sections we consider the calculation of the macroscopic swarm transport properties, in the gaseous and liquid xenon environments, from the microscopic cross-sections, modified by the screening and coherent scattering effects discussed above. We first discuss a multi-term solution of Boltzmann's equation in Section II, using the calculation of the elastic scattering cross-section for electrons in dilute gaseous xenon via the Dirac-Fock scattering equations in Section III. We determine the xenon pair-correlator at the xenon triple point in Section IV A using a Monte-Carlo simulation of a Lennard-Jones with parameters fitted from experimental data in the gas phase and compare the results with previous calculations. The pair-correlator allows us to determine an effective liquid scattering cross-section for xenon (see Section IV B), in the manner outlined in Boyle et al. [1]. The application of these cross-sections to determine macroscopic transport properties via kinetic theory is also outlined in Section II. We present the results of our transport calculations in Section V. Initially in Section V A we consider only electrons in gas-phase xenon, and we compare the reduced mobility and characteristic energies with swarm experiment measurements for a range of fields. Electrons in liquid-phase xenon are then considered in Section V B. The impact of anisotropic scattering and validity of the two-term approximation is also investigated, and we highlight the importance of using a multi-term framework when solving Boltzmann's equation accurately. Finally, we discuss a scaling procedure to adapt other gas-phase cross-section sets, such as those compiled from various theoretical and experimental sources, to the liquid phase in Section V C, and compare the transport properties. Throughout this paper we will make use of atomic units ($m_e = e = a_0 = \hbar = 1$) unless otherwise specified.

II. MULTI-TERM SOLUTION OF BOLTZMANN'S EQUATION

A dilute swarm of electrons moving through gaseous or liquid xenon, subject to an external electric field E, can be described by the solution of the Boltzmann's equation for the phase-space distribution function $f(\boldsymbol{r}, \boldsymbol{v}, t)$ [21]:

$$\frac{\partial f}{\partial t} + \boldsymbol{v} \cdot \nabla f + \frac{e\boldsymbol{E}}{m_e} \cdot \frac{\partial f}{\partial \boldsymbol{v}} = -J(f), \tag{1}$$

where $\boldsymbol{r}$, $\boldsymbol{v}$ and e denote the position, velocity and charge of the electron respectively. The collision operator $J(f)$ accounts for all the necessary collision types and interactions between the electrons of mass m_e and the background medium. In this paper we will only consider reduced electric field strengths E/N (where N is the number density of the background material) such that there is no significant contribution from excitation collisions in xenon.

In swarm experiments only a few macroscopic variables can be controlled and/or measured [22]. The most commonly reported transport quantities for electrons in liquids are the mobility μ ($= W/E$, where W is drift velocity), and the transverse and longitudinal characteristic energies, D_T/μ and D_L/μ respectively. As shown in [1], we can calculate these coefficients through multi-term spherical harmonic representations of the necessary velocity distribution functions:

$$F(\boldsymbol{v}) = \sum_{l=0}^{\infty} F_l(v) P_l^0(\cos\theta) \ , \tag{2}$$

$$F^{(L)}(\boldsymbol{v}) = \sum_{l=0}^{\infty} F_l^{(L)}(v) P_l(\cos\theta) \ , \tag{3}$$

and

$$F^{(T)}(\boldsymbol{v}) = \sum_{l=0}^{\infty} F_l^{(T)}(v) P_l^1(\cos\theta) \ . \tag{4}$$

Note that θ denotes the angle relative to the electric field direction (taken to be the z-axis) and $P_l^m(\cos\theta)$ are associated Legendre polynomials. The Boltzmann equation can be re-written as the following hierarchy of equations for these expansion coefficients:

$$J^l F_l + \frac{l+1}{2l+3} a \left(\frac{\partial}{\partial v} + \frac{l+2}{v} \right) F_{l+1} + \frac{l}{2l-1} a \left(\frac{\partial}{\partial v} - \frac{l-1}{v} \right) F_{l-1} = 0, \tag{5}$$

$$J^l F_l^{(L)} + \frac{l+1}{2l+3} a \left(\frac{\partial}{\partial v} + \frac{l+2}{v} \right) F_{l+1}^{(L)} + \frac{l}{2l-1} a \left(\frac{\partial}{\partial v} - \frac{l-1}{v} \right) F_{l-1}^{(L)} = v \left(\frac{l+1}{2l+3} F_{l+1} + \frac{l}{2l-1} F_{l-1} \right), \tag{6}$$

and

$$J^l F_l^{(T)} + \frac{l+2}{2l+3} a \left(\frac{\partial}{\partial v} + \frac{l+2}{v} \right) F_{l+1}^{(T)} + \frac{l-1}{2l-1} a \left(\frac{\partial}{\partial v} - \frac{l-1}{v} \right) F_{l-1}^{(T)} = v \left(\frac{F_{l-1}}{2l-1} - \frac{F_{l+1}}{2l+3} \right), \tag{7}$$

where the J^l represent the Legendre projections of the collision operator detailed below and $a = eE/m_e$. We enforce the normalisation condition:

$$4\pi \int_0^\infty F_0(v) v^2 dv = 1 \, . \tag{8}$$

The solution of this hierarchy of equations then yields the mobility:

$$\mu = \frac{1}{E} \frac{4\pi}{3} \int_0^\infty v^3 F_1 dv, \tag{9}$$

and the characteristic energy:

$$D_{(L,T)} = \frac{4\pi}{3} \int_0^\infty v^3 F_1^{(L,T)} dv \, . \tag{10}$$

Note, this theory avoids the traditional two-term approximation used in electron transport in liquids [12, 16, 23], and is a true multi-term solution of Boltzmann's equation, whereby the upper bound in each of the l-summations is truncated at a value $l_{\max}$, and this value is incremented until some convergence criteria is met on the distribution function or its velocity moments.

We only consider low-energy elastic scattering in this study. Hence, the collision operator appearing in (1), which describes the rate of change of the distribution function due to interactions with the background material, will include elastic collisions only. For the liquid systems considered here, the de Broglie wavelength of the electron is often of the order of the average inter-particle spacing $\sim N^{-1/3}$. In this energy regime, the electron is best viewed as a wave that simultaneously interacts with multiple scattering centres that comprise the medium. For liquid xenon, the average interparticle spacing is approximately 2.6 Å, implying that "low" energies are those less than ~ 0.5 eV, which is several orders of magnitude larger

than the thermal energy of ~ 0.014 eV. The interaction potential is then modified from the dilute gas phase as discussed in Section IV B.

The Legendre projections of the elastic collision operator, in the small mass ratio limit, accounting for coherent scattering, are given by:

$$J^0\left(\Phi_l\right) = \frac{m_e}{Mv^2}\frac{d}{dv}\left\{v\nu_1(v)\left[v\Phi_l + \frac{kT}{m_e}\frac{d}{dv}\Phi_l\right]\right\} \tag{11}$$

$$J^l\Phi_l = \tilde{\nu}_l(v)\Phi_l \qquad \text{for } l{\geq}1, \tag{12}$$

where M is the mass of a xenon atom, $\Phi_l = \left\{F_l, F^{(L)}, F^{(T)}\right\}$ and

$$\nu_l(v) = Nv2\pi\int_0^\pi \sigma(v,\chi)\left[1 - P_l(\cos\chi)\right]\sin\chi d\chi, \tag{13}$$

is the binary transfer collision frequency in the absence of coherent scattering effects with $\sigma(v,\chi)$ the differential scattering cross-section. In addition,

$$\tilde{\nu}_l(v) = Nv\left(2\pi\int_0^\pi \Sigma(v,\chi)\left[1 - P_l(\cos\chi)\right]\sin\chi d\chi\right). \tag{14}$$

are the structure-modified higher-order collision frequencies that account for coherent scattering through:

$$\Sigma(v,\chi) = \sigma(v,\chi)\; S\left(\frac{2m_e v}{\hbar}\sin\frac{\chi}{2}\right), \tag{15}$$

which represents an effective differential cross-section. S is the static structure factor, which can be determined from the pair-correlator as discussed in Section IV B. In what follows we also define the momentum transfer cross-sections without and with coherent scattering via $\nu_1(v) = Nv\sigma_m(v)$ and $\tilde{\nu}_1(v) = Nv\Sigma_m(v)$, respectively.

III. SCATTERING OF ELECTRONS BY XENON GAS

The theoretical procedures used in this paper, to describe the elastic scattering of electrons from xenon atoms at low energies, are essentially the same as those used in Boyle et al. [1] for electron scattering from argon. We thus present only a short summary here and refer the reader to reference [1] for more details.

In the pure elastic scattering energy region, only two interactions need to be considered, namely polarization and exchange. The polarization interaction is accounted for by means of

a long-range multipole polarization potential, while the exchange interaction is represented by a short-range non-local potential formed by antisymmetrizing the total scattering wavefunction. The scattering of the incident electrons, with wavenumber k, by xenon atoms can then be described in the gaseous phase by the integral equation formulation of the partial wave Dirac-Fock scattering equations (see Chen et al. [24] for details).

In matrix form, these equations can be written as:

$$\begin{pmatrix} f_\kappa(r) \\ g_\kappa(r) \end{pmatrix} = \begin{pmatrix} v_1(kr) \\ v_2(kr) \end{pmatrix} + \frac{1}{k} \int_0^r \mathrm{d}x\, G(r,x) \left[U(x) \begin{pmatrix} f_\kappa(x) \\ g_\kappa(x) \end{pmatrix} - \begin{pmatrix} W_Q(\kappa;x) \\ W_P(\kappa;x) \end{pmatrix} \right], \tag{16}$$

where the local potential $U(r)$ is given by the sum of the static and local polarization potentials i.e.,

$$U(r) = U_\mathrm{s}(r) + U_\mathrm{p}(r) \tag{17}$$

and $W_P(\kappa;r)$ and $W_Q(\kappa;r)$ represent the large and small components of the exchange interaction.

The precise form of these exchange terms is given in equation (5) of Boyle et al. [1]. In particular, the polarization potential $U_\mathrm{p}(r)$ in equation (17) was determined using the polarized orbital method [25] and contained several static multipole terms as well as the corresponding dynamic polarization term [26, 27]. In total, the potential $U(r)$ contained all terms up to and including those that behave as r^{-16} asymptotically.

In equation (16), $f_\kappa(r)$ and $g_\kappa(r)$ are the large and small components of the scattering wavefunction. Here the quantum number κ is related to the total and orbital angular momentum quantum numbers j and l according to $\kappa = -l-1$ when $j = l + 1/2$ (spin-up) and $\kappa = l$ when $j = l - 1/2$ (spin down). Furthermore, $G(r,x)$ is the free particle Green's function given in equations (23) and (24a,b) of Chen et al. [24]. The kinetic energy ϵ of the incident electron and its wavenumber k are related by:

$$k^2 = \frac{1}{\hbar^2 c^2}\, \epsilon \left(\epsilon + 2mc^2\right), \tag{18}$$

where c is the velocity of light which, in atomic units, is given by $c = 1/\alpha$ where α is the fine-structure constant.

In the integral equation formulation, the scattering phase shifts can be determined from the asymptotic form of the large component of the scattering wavefunction i.e.,

$$f_\kappa(r) \xrightarrow[r\to\infty]{} A_\kappa\, \hat{j}_l(kr) - B_\kappa\, \hat{n}_l(kr), \tag{19}$$

where $\hat{j}_l(kr)$ and $\hat{n}_l(kr)$ are the Riccati-Bessel and Riccati-Neumann functions while the constants A_κ and B_κ are defined in equations (7) and (8) of Boyle et al. [1] . The partial wave phase shifts are then given by:

$$\tan\delta^{\pm}(k) = \frac{B_\kappa}{A_\kappa}, \tag{20}$$

where the $\delta^{\pm}$ are the spin-up $(+)$ and spin-down $(-)$ phase shifts. The total elastic and momentum transfer cross-sections are given, in terms of these phase shifts, by:

$$\sigma_{\rm el}(k^2) = \frac{4\pi}{k^2}\sum_{l=0}^{\infty}\Big\{(l+1)\,\sin^2\delta_l^+(k) + l\,\sin^2\delta_l^-(k)\Big\} \tag{21}$$

and

$$\sigma_{\rm mt}(k^2) = \frac{4\pi}{k^2}\sum_{l=0}^{\infty}\Big\{\frac{(l+1)(l+2)}{2l+3}\,\sin^2\big(\delta_l^+(k)-\delta_{l+1}^+(k)\big) + \frac{l(l+1)}{2l+1}\,\sin^2\big(\delta_l^-(k)-\delta_{l+1}^-(k)\big) + \frac{(l+1)}{(2l+1)(2l+3)}\,\sin^2\big(\delta_l^+((k)-\delta_{l+1}^-(k)\big)\Big\}. \tag{22}$$

Analytic fits of the above momentum-transfer cross-section (and for other noble gases) are given in McEachran and Stauffer 2014 [28] to aid in plasma modelling calculations.

In Figure 1, the momentum transfer cross-section in the gas-phase is compared to the cross-section recommended by Biagi [29] from the "Magboltz" Boltzmann equation solver. The Biagi elastic momentum transfer cross-section has been constructed from the unpublished analysis of Elford, fitting to the available drift velocity and diffusion coefficients [30]. It is often considered the reference cross-section for electron-xenon interactions in the gas phase. Our momentum transfer cross-section gives good qualitative agreement with the Biagi reference cross-section, but generally somewhat over-estimates the value. The location and depth of the Ramsauer minima, however, agrees closely.

IV. SCATTERING OF ELECTRONS BY XENON LIQUID

A. Xenon pair correlation

The only measurements of the liquid phase xenon structure factor that are known to us, are by Becchi and Magli [31] for $T = 274.7$ K and $N = 8.86\times10^{21}\,\mathrm{cm}^{-3}$, near to the critical point of $T = 289.72$ K. In order to obtain a structure factor at the lower

temperature of $T = 165$ K and $N = 14.2{\times}10^{22}\,\mathrm{cm}^{-3}$, where the transport measurements have been performed, we have used a Lennard-Jones model, calibrated to the high temperature structure factor, to construct a low temperature structure factor by performing Monte-Carlo simulations of the fluid.

The Lennard-Jones fluid has a pair-wise potential given by:

$$V(r) = 4\epsilon_{LJ}\left[\left(\frac{r}{\sigma_{LJ}}\right)^{12} - \left(\frac{r}{\sigma_{LJ}}\right)^{6}\right], \tag{23}$$

with the characteristic energy ϵ_{LJ} and length scale σ_{LJ}. Often, this potential is truncated to a range of $r_{\mathrm{trunc}} = 2.5\,\sigma_{LJ}$ but we work with an effectively untruncated potential by extending r_{trunc} to the system size $r_{\mathrm{trunc}} = L/2$. For the truncated potential, Atrazhev et al [32] have used values of $\epsilon_{LJ}/k_B = 299\,\mathrm{K}$ and $\sigma_{LJ} = 4.05$ but, by comparing to the experimental data of reference [31], we find a better fit for our untruncated model by matching the critical temperature of the Lennard-Jones model ($k_B T_{\mathrm{crit}} = 1.312\,\epsilon_{LJ}$ [33]) to the measured value of 289.72 K leaving us instead with $\epsilon_{LJ}/k_B = 220.83$ K. Given this value, the best fit to the data of reference [31] is $\sigma_{LJ} = 3.86$. We then use these parameters to obtain the pair-correlator at the desired temperature of $T = 165$ K. A plot of the various structure factors is shown in figure 2, where we compare with the structure factor calculated from the truncated potential in the paper of Atrazhev et al. [32].

B. Liquid xenon cross-section

In order to capture the major effects of increasing the number density of the fluid system, we include two modifications to the gas scattering potentials due to: a) the screening of the long-range polarization potential, and b) the influence of the particles in the medium bulk. The procedure outlined in this section closely follows that of references [1, 16]. We summarize the steps here.

Firstly, the effective charge-multipole polarization potential acting between the electron and the induced multipole of an individual atom is reduced by the presence of the induced multipoles in the surrounding atoms, which produces a screening effect. Using the (isotropic) pair-correlator for xenon, $g(r)$, determined in Section IV A, we have self-consistently calculated the screening function $f(r)$ for an electron located at position r via:

$$f(r) = 1 - \pi N \int_0^\infty ds \; \frac{g(s)}{s^2} \int_{|r-s|}^{r+s} dt \; \Theta\left(r,s,t\right) \frac{\alpha(t) f(t)}{t^2}, \tag{24}$$

which has been represented in bipolar coordinates, s and t, and where

$$\Theta\left(r,s,t\right) = \frac{3}{2} \frac{\left(s^2+t^2-r^2\right)\left(r^2+t^2-s^2\right)}{s^2} + \left(r^2+t^2-s^2\right), \tag{25}$$

arises due to the form of the electric field of a dipole. The screening function is used to determine the screened polarization potential, $\tilde{U}_p(r)$, of an electron with one atom in a dense fluid,

$$\tilde{U}_p(r) = f(r) U_p(r). \tag{26}$$

Secondly, the direct interaction of the electrons with other atoms in the bulk is significant in a dense system, even when the electron is very close to the focus atom. By following the procedure of Lekner [34], we construct an effective potential, $U_{\text{eff}} = U_1 + U_2$, where U_1 describes the direct (screened) interaction of the electrons and the target atom, and where U_2 describes the collective interaction of the electron with the rest of the bulk atoms. We approximate U_2 by an ensemble average of the bulk, i.e.,

$$U_2(r) = \frac{2\pi N}{r} \int_0^\infty dt \; U_1(t) \int_{|r-t|}^{r+t} ds \; sg(s). \tag{27}$$

We note that taking the ensemble average has the advantage of enforcing spherical symmetry of the total effective potential U_{eff}.

Since, in a dense system, the electron is never in effectively free space, a different measure of the volume "owned" by the focus atom is required. It is natural to define the distance of first turning point of the potential U_{eff}, which is denoted by r_m, as the spherical distance under the influence of the focus atom. Hence we can say that a single collision event takes place when an electron enters and leaves the radius r_m of a single atom. In order to calculate the phase shift at the distance r_m rather than infinity, we have set the upper limits of equations (7) and (8) of Boyle et al. [1] for A_κ and B_κ to be r_m.

The full differential elastic scattering cross-section for the gas and liquid phases (with and without coherent scattering) are displayed in Figure 3. For the dilute gas phase, we observe the presence of a forward-peaked minimum in the range 0.2–1 eV, below which the differential cross-section is essentially isotropic. This minimimun is the well-known Ramsauer

minimimun which occurs in a number of electron-atom gas-phase cross-sections. At energies above the minimun, the differential cross-section demonstrates increased magnitude and also enhanced anisotropy, with peaks in the forward- and back-scattering directions. When the modification due to screening and interactions from the liquid bulk are included, we observe the suppression of the Ramsauer minimum and a removal of the forward peak for low and moderate energies. At higher energies, the liquid differential cross-section becomes similar both qualitatively and quantitatively to the gas phase cross-section. When the liquid phase differential cross-section is combined with the static structure factor accounting for coherent scattering effects, the resulting differential cross-section $\Sigma(\epsilon, \chi)$ takes on a completely different qualitative structure. At low energies, the differential scattering cross-section has been further reduced in magnitude at all scattering angles. At higher energies the forward-scattering has been reduced, while the back-scattering peak remains essentially unaffected.

The momentum transfer cross-sections corresponding to the differential scattering cross-sections in Figure 3 are displayed in Figure 4, along with the cross-sections from Atrazhev et al. [32]. The comments made regarding the differential scattering cross-sections are once again reflected here. The Ramsauer minimum observed in the gas-phase is completely suppressed in the liquid-phase, and there is a large reduction in the magnitude of the cross-sections when the screening and liquid effects are included, and again when coherent scattering effects are included. At higher energies, the liquid-phase cross-sections approach the gas-phase values, with some additional oscillatory structure evident when coherent scattering is included. The cross-sections of Atrazhev et al. [32] have been calculated using a similar formalism, but with a pseudo-potential that replaces the short-range part of the interaction by a boundary condition that reproduces the expected scattering length in the gas-phase. Their cross-sections are qualitatively similar to ours, but are consistently smaller in magnitude over the range of energies considered. We attribute these differences to our treatment of the static and exchange parts of the potential, for both the focus and surrounding atoms, as well as the inclusion of a full multipole polarization potential.

V. RESULTS

One of the key functions of modern-day swarm experiments is to assess the completeness and accuracy of cross-section [35–38] sets. Swarm experiments are many-scattering

experiments, where there is a balance established between the number of particles and the momentum and energy transfers occurring. In the following sections we consider the calculation of the macroscopic swarm transport properties in the gaseous and liquid environments from the microscopic cross-sections. Particular attention is given to investigating the validity of the two-term approximation in our calculations, and we compare these with the full multi-term results. In Section V C, we introduce a simple scaling algorithm to adapt any gas-phase cross-section to the liquid-phase based on the our *ab initio* scattering calculations.

A. Electrons in gaseous xenon

The calculated reduced mobility and characteristic energies using the gas-phase cross-sections detailed in Section III and the reference cross-sections of Biagi [30] are presented in Figure 5. They are compared against various experimental data for xenon gas [39, 40]. We restrict ourselves to the reduced electric fields of less than 1 Td, to ensure we are in the energy regime where only elastic scattering is operative. For the gas calculations, using the present cross-sections, we observe agreement to within 30% or better for both the reduced mobility and the transverse characteristic energy over the range of the reduced fields considered. These errors decrease to 5% or better for the transverse characteristic energy, above the field region where the transport properties rapidly increase. This can be compared with the Biagi [30] cross-section calculations, which demonstrate agreement to within 10% or better (generally less than 5%) for reduced mobility and transverse characteristic energy. Although the experimental longitudinal characteristic energies exhibit larger variation and error than the transverse counterpart, our calculated energies using the present cross-sections and those of Biagi [30] appear to give good agreement. The major difference between the transport calculations using the two different cross-sections is in the turning point of the longitudinal characteristic energy profile: our ab initio cross-sections cause a turning point at slightly higher reduced electric field strengths than the experiment, whereas the Biagi cross-sections is consistent with the experimental measurements.

In a direct reflection of our increased momentum transfer cross-section, as compared to the reference, the transverse characteristic energy and reduced mobility generally underestimate the experimental measurements [39, 40]. The increased momentum transfer tends to increase the randomization of the electron's direction during a collision, which reduces the field's

ability to efficiently pump energy into the system. It is no surprise that the Biagi cross-section gives closer agreement between calculation and experiment, since it is informed by experimental swarm measurements and was not from an *ab initio* theory.

B. Electrons in liquid xenon

In Figure 6 the reduced mobility and characteristic energies are now compared in both the gaseous and liquid phases. The transport coefficients are presented against reduced electric fields so that any linear dependence on density (as occurs in the dilute-gas limit) has been removed, and so we have a true comparison of the gaseous and liquid phases. Qualitatively, for a given reduced field in the low-energy regime, we observe that the reduced mobility and transverse characteristic energy in the liquid phase are both significantly larger, often by several orders of magnitude over the gaseous phase. In our investigations of electrons in liquid argon [1], the transverse characteristic energy in the liquid phase was instead smaller than in the gaseous phase. The longitudinal characteristic energy is generally larger for reduced electric field strengths of less than ~ 0.2 Td, but smaller for the higher electric field strength considered. Our calculations using the ab-initio theory are accurate to within 25% for the mobility (generally less than 15%) and 25% for the transverse characteristic energy. These are of similar magnitude to those for the gas phase.

Although the differential scattering cross-sections for Xe displayed an enhanced anisotropic nature in the liquid phase over that in the gas phase, the impact of this anisotropy on the velocity distribution function was not particularly significant here. The errors associated with the two-term approximation ($l_{\max} = 1$) to the velocity distribution function are displayed in Figure 7. In the gaseous and liquid phases there are differences as large as 10% and 40% respectively, in the transverse characteristic energies. The errors associated with the longitudinal characteristic energies was less than 0.1% for both the gas and liquid phases, and hence were omitted from Figure 7.

C. Rescaling gas phase cross-sections

It was noted in Section V A that our gas phase momentum-transfer cross-section overestimates the reference cross-section of Biagi [29, 30], the latter of which is shown to produce

transport data accurate to within 10% of the experimental data, compared with 30% for the current *ab-initio* theory. In order to utilize the apparent enhanced accuracy associated with the experimental cross-section, we postulate a method of extracting the explicit liquid-based effects from the theory and applying it to the experimentally measured cross-section. The ratio of the liquid to gas phase cross-section using our formalism gives an energy dependent scaling for the importance of screening and coherent scattering. Let us define a scaling factor, $\xi_l(v)$, such that:

$$\xi_l(v) = \frac{\tilde{\nu_l}(v)}{\nu_l(v)}, \tag{28}$$

where these ν correspond to our scattering calculations using the Dirac-Fock equations described in Section III and IV B respectively. We can then build an effective liquid-phase momentum-transfer cross-section based on the Biagi [30] reference data, $\Sigma_m^{Biagi}(v)$, via:

$$\Sigma_m^{Biagi}(v) = \xi(v)\sigma_m^{Biagi}(v), \tag{29}$$

where $\sigma_m^{Biagi}(v)$ is the Biagi recommended gas-phase cross-section [30]. It should be noted that, due to the lack of differential cross-section information for the Biagi set, only a two-term approximation can be used here, i.e. only the momentum transfer cross-section is known. The effective Biagi liquid momentum transfer cross-section is shown in Figure 8. The method is similar in spirit to the procedure proposed in reference [41], though scaling was done with respect to the transport coefficients rather than the cross-sections.

The characteristic energies and reduced mobility calculated using the effective Biagi liquid momentum transfer cross-section is shown in Figure 9, along with the previous calculations considered in this manuscript. It appears that this result gives a slightly better agreement with experiment for the reduced mobilities at low field strengths i.e., errors within 20%, while it is no worse for the transverse characteristic energiy. The biggest improvements occur at the low electric field strengths, where the errors are effectively half that of the *ab initio* approach.

VI. CONCLUSIONS

We have presented an *ab-initio* treatment of electron scattering and transport in liquid xenon. There are no free parameters in this calculation, and hence the agreement to within

25% in the mobility and the transverse characteristic energy in the reduced field range 10^{-4}–1 Td is considered satisfactory.Given that, in the dilute gas phase, agreement to within 30% for the mobility and transverse characteristic energy transport coefficients was achieved, with the current scattering calculations, this gives confidence that the majority of the essential physics for considering high mobility noble liquids is present in the theory. A scaling factor formed from the ratio of the calculated liquid to gas phase cross-sections, was postulated to encompass the "liquid"-based effects, enabling more accurate gas-phase cross-sections derived from experiment to be translated to liquid-phase cross-sections. Subsequent enhancements in the accuracy of the transport coefficient calculations were achieved, with the mobility errors reduced to 20% and and even bigger improvement displayed for the lowest fields considered.

ACKNOWLEDGMENTS

This work was supported in part by the Australian Research Council through its Discovery Program scheme. M. J. B. and S. J. B. acknowledge University Malaysia for their "Icon Professor" appointments, while R. D. White thanks Prof. K Ratnavelu for some financial support through the University Malaysia grant UMRP11A-13AFR. S. D. acknowledges support from MPNTRRS Projects OI171037 and III41011.

[1] G. J. Boyle, R. P. McEachran, D. G. Cocks, and R. D. White, J. Chem. Phys. **142**, 154507 (2015).

[2] C. Regenfus and the ArDM collaboration, J. Phys. Conf. Ser. **203**, 012024 (2010).

[3] E. Aprile and T. Doke, Rev. Mod. Phys. **82**, 2053 (2010).

[4] E. Aprile, J. Angle, F. Arneodo, L. Baudis, A. Bernstein, A. Bolozdynya, et al, Astropart. Phys. **34**, 679 (2011).

[5] G. J. Alner, H. M. Araújo, A. Bewick, C. Bungau, B. Camanzi, M. J. Carson, et al, Astropart. Phys. **28**, 287 (2007).

[6] B. Baller, C. Bromberg, N. Buchanan, F. Cavanna, H. Chen, E. Church, et al, J. Instrum. **9**, T05005 (2014).

[7] S. Amerio, S. Amoruso, M. Antonello, P. Aprili, M. Armenante, F. Arneodo, et al, Nucl. Instr. Meth. Phys. Res. A **527**, 329 (2004).

[8] C. Rubbia, M. Antonello, P. Aprili, B. Baibussinov, M. Baldo Ceolin, L. Barzé, et al, J. Instrum. **6**, P07011 (2011).

[9] The ATLAS collaboration, J. Instrum. **9**, P07024 (2014).

[10] N. Gee and G. R. Freeman, Can. J. Chem. **64**, 1810 (1986).

[11] G. Braglia and V. Dallacasa, Phys. Rev. A **26**, 902 (1982).

[12] A. F. Borghesani, IEEE Transactions on Dielectrics and Electrical Insulation **13**, 492 (2006).

[13] Y. Sakai, Journal of Physics D: Applied Physics **40**, R441 (2007).

[14] R. D. White and R. E. Robson, Phys. Rev. Lett. **102**, 230602 (2009).

[15] E. E. Kunhardt, Physical Review B **44**, 4235 (1991).

[16] M. H. Cohen and J. Lekner, Physical Review **158**, 305 (1967).

[17] V. M. Atrazhev and I. T. Iakubov, Journal of Physics C: Solid State Physics **14**, 5139 (1981).

[18] V. Atrazhev and I. Timoshkin, Physical Review B **54**, 11252 (1996).

[19] R. D. White and R. E. Robson, Physical Review E **84**, 031125 (2011).

[20] R. D. White, R. E. Robson, B. Schmidt, and M. Morrison, Journal of Physics D: Applied Physics **36**, 3125 (2003).

[21] L. Boltzmann, Wein. Ber. **66**, 275 (1872).

[22] L. G. H. Huxley and R. W. Crompton, *The Drift and Diffusion of Electrons in Gases* (Wiley, New York, 1974).

[23] Y. Sakai, Journal of Physics D: Applied Physics **40**, R441 (2007).

[24] S. Chen, R. P. McEachran, and A. D. Stauffer, J. Phys. B **41**, 025201 (2008).

[25] R. P. McEachran, A. D. Stauffer, A. G. Ryman, and D. L. Morgan, J. Phys. B **10**, 663 (1977).

[26] R. P. McEachran and A. D. Stauffer, J. Phys. B **23**, 4605 (1990).

[27] D. J. R. Mimnagh, R. P. McEachran, and A. D. Stauffer, J. Phys. B **26**, 1727 (1993).

[28] R. P. McEachran and A. D. Stauffer, Eurl. Phys. J. **68**, 153 (2014).

[29] S. F. Biagi, "Biagi database," www.lxcat.net (2014), accessed 30 April, 2014.

[30] M. C. Bordage, S. F. Biagi, L. L. Alves, K. Bartschat, S. Chowdhury, L. C. Pitchford, G. J. M. Hagelaar, V. P. Morgan, and O. Zatsarinny, J. Phys. D: Appl. Phys. **46**, 334003 (2013).

[31] M. Becchi and R. Magli, Physica B: Condensed Matter **234**, 316 (1997).

[32] V. M. Atrazhev, A. V. Berezhnov, D. O. Dunikov, and I. V. Chernysheva, in *IEEE International Conference on Dielectric Liquids* (2005) pp. 329–332.

[33] J. Pérez-Pellitero, P. Ungerer, G. Orkoulas, and A. D. Mackie, Journal of Chemical Physics **125**, 1 (2006).

[34] J. Lekner, Physical Review **158**, 103 (1967).

[35] G. Boyle, M. Casey, R. White, and J. Mitroy, Physical Review A **89**, 022712 (2014).

[36] G. J. Boyle, M. J. E. Casey, R. D. White, Y. Cheng, and J. Mitroy, Journal of Physics D: Applied Physics **47**, 345203 (2014).

[37] J. de Urquijo, E. Basurto, a. M. Juárez, K. F. Ness, R. E. Robson, M. J. Brunger, and R. D. White, The Journal of chemical physics **141**, 014308 (2014).

[38] R. D. White, M. J. Brunger, N. a. Garland, R. E. Robson, K. F. Ness, G. Garcia, J. de Urquijo, S. Dujko, and Z. L. Petrović, The European Physical Journal D **68**, 125 (2014).

[39] T. Koizumi, E. Shirakawa, and I. Ogawa, J. Phys. B: At. Mol. Phys. **19**, 2331 (1986).

[40] J. L. Pack, R. E. Voshall, A. V. Phelps, and L. E. Kline, J. Appl. Phys. **71**, 5363 (1992).

[41] G. J. Boyle, R. D. White, R. E. Robson, S. Dujko, and Z. Lj Petrović, New Journal of Physics **14**, 045011 (2012).

[42] J. Yarnell, M. Katz, R. Wenzel, and S. Koenig, Phys. Rev. A **7**, 2130 (1973).

[43] E. Shibamura, K. Masuda, and T. Doke, in *8th Workshop on Electron Swarms* (1984).

[44] S. S. S. Huang and G. R. Freeman, J. Chem. Phys. **47**, 1355 (1978).

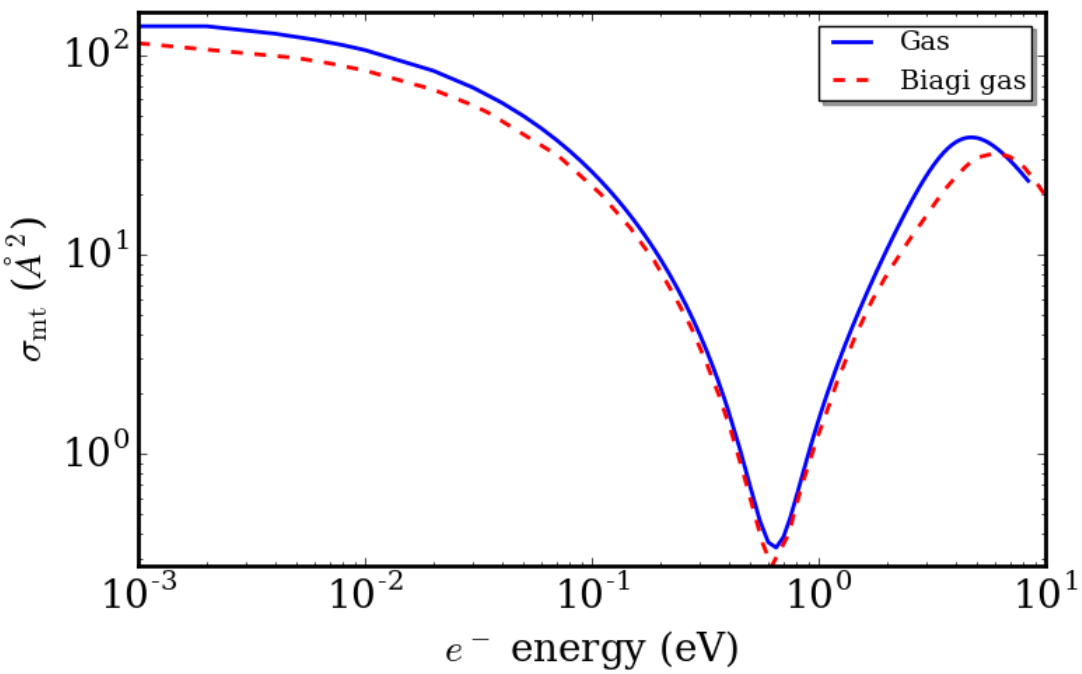

Figure 1. The current momentum transfer cross-sections in the gas-phase (Gas), and the reference momentum transfer cross-section of Biagi [30] (Biagi gas).

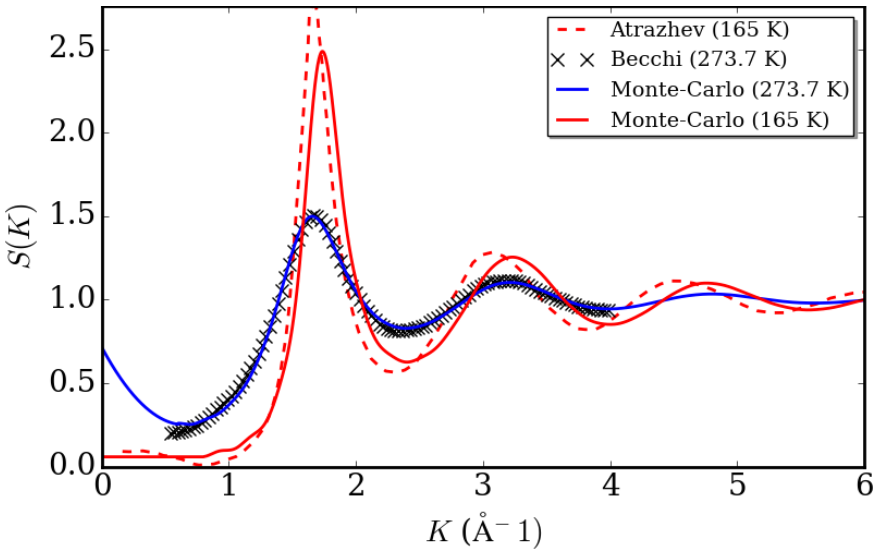

Figure 2. Xenon structure factors. The crosses represent the Becchi measurements [31] and the solid blue lines are our Monte-Carlo simulations of the Lennard-Jones fluid at a high temperature near the critical point of 274.7 K. The solid green line represents the structure factor at 165 K that we use in this paper and the dashed green line shows the rescaled measurements from argon experimental data [42] used by reference [32].

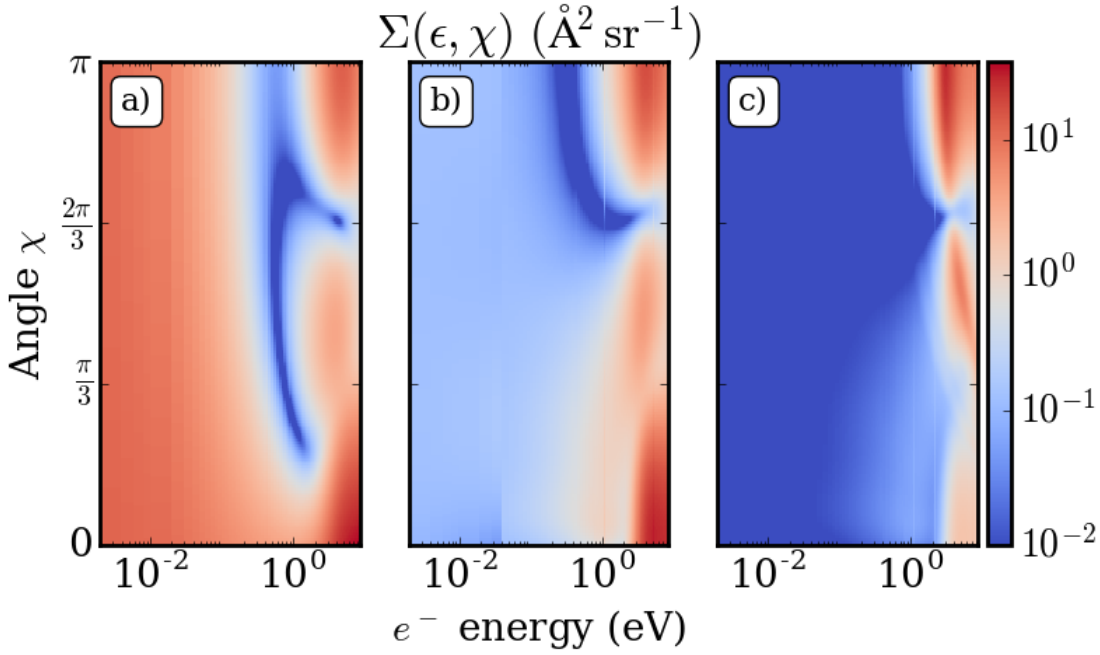

Figure 3. Current differential cross-sections, $\Sigma(\epsilon, \chi)$., in square angstroms for electrons in Xe for a) dilute gas phase, b) effective liquid phase including screening effects, and c) liquid phase including coherent scattering effects.

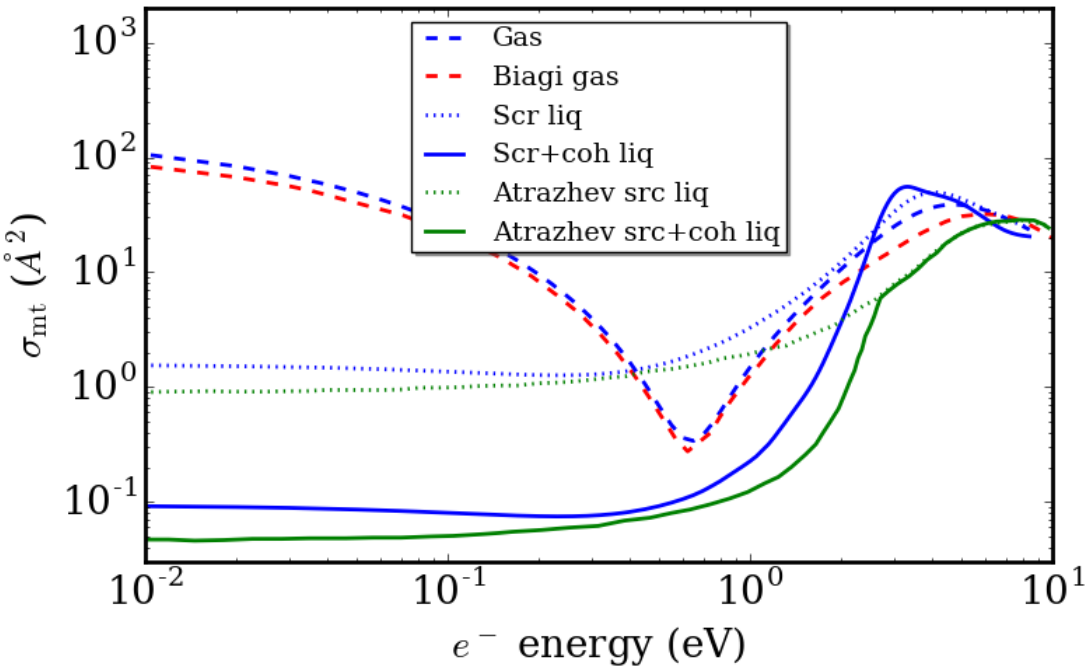

Figure 4. The current momentum transfer cross-sections in the gas-phase (Gas; Biagi gas), liquid-phase (Scr liq, Atrazhev scr liq) and including their modifications when coherent scattering effects are included (Scr + coh liq, Atrazhev scr + coh liq). A detailed description of the Atrazhev et al. cross-section calculations is given in reference [32].

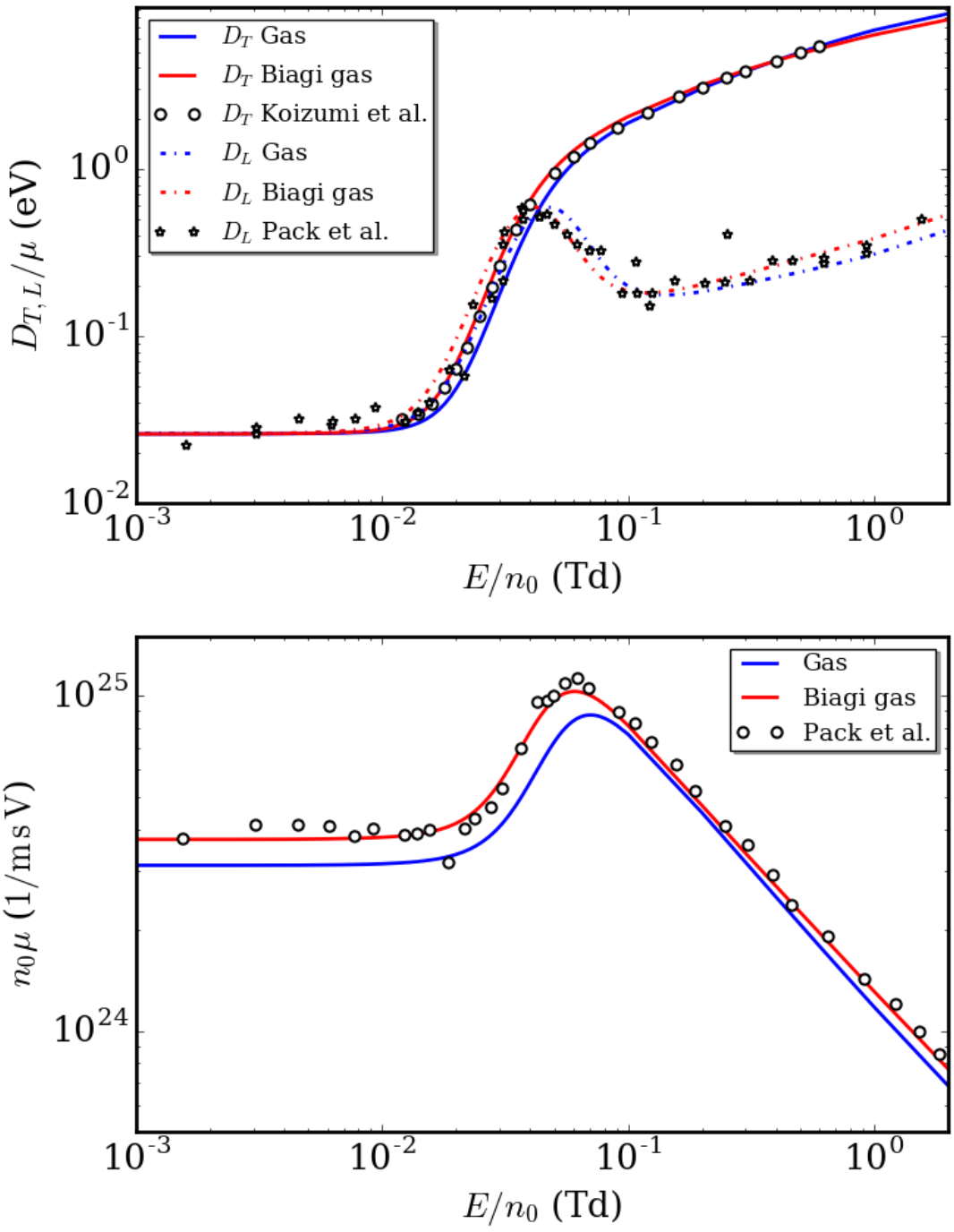

Figure 5. The transverse (D_T/μ) and longitudinal (D_L/μ) characteristic energies (top) and reduced mobility ($n_0\mu$) (bottom) of electrons in gaseous xenon, calculated using the current potentials and associated cross-sections detailed in Section III (Gas), and the recommended cross-section of Biagi [30] (Biagi gas), and compared with available experimental data (Koizumi et al. [39] at 300 K; Pack et. al [40] at 300 K;). The background xenon gas for the calculations was fixed at 300 K.

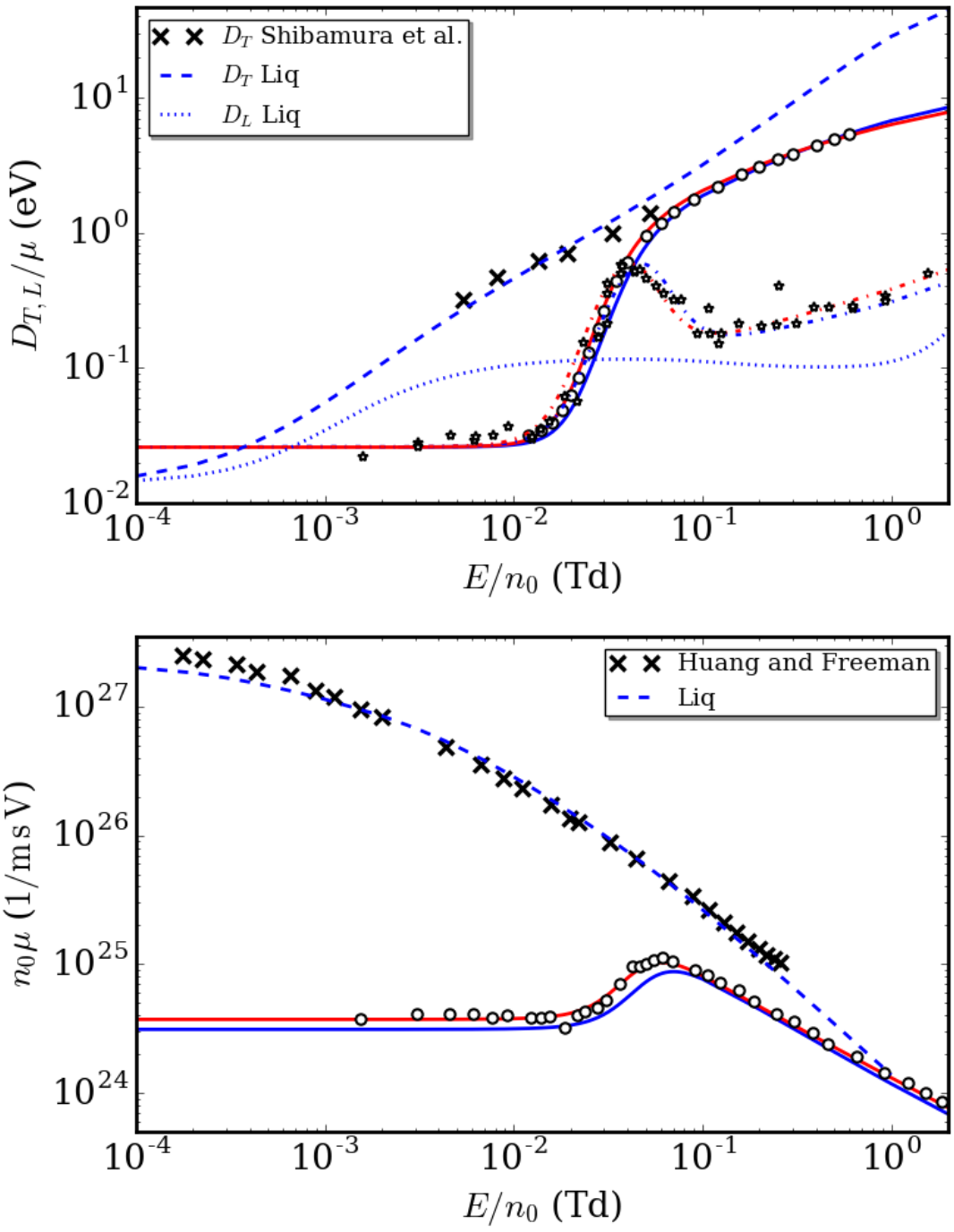

Figure 6. Comparison of the transverse (D_T/μ) and longitudinal (D_L/μ) characteristic energies (top) and reduced mobilities ($n_0\mu$) (bottom) in gaseous and liquid xenon, with those calculated from the various approximations to the cross-sections. Experimental data (Liquid phase: Shibamaru et al. [43] at 165K; Huang and Freeman [44] at 163 K). The current liquid-phase cross-sections (Liq) have been calculated including coherent scattering effects. All other profiles are the same as given in Figure 5.

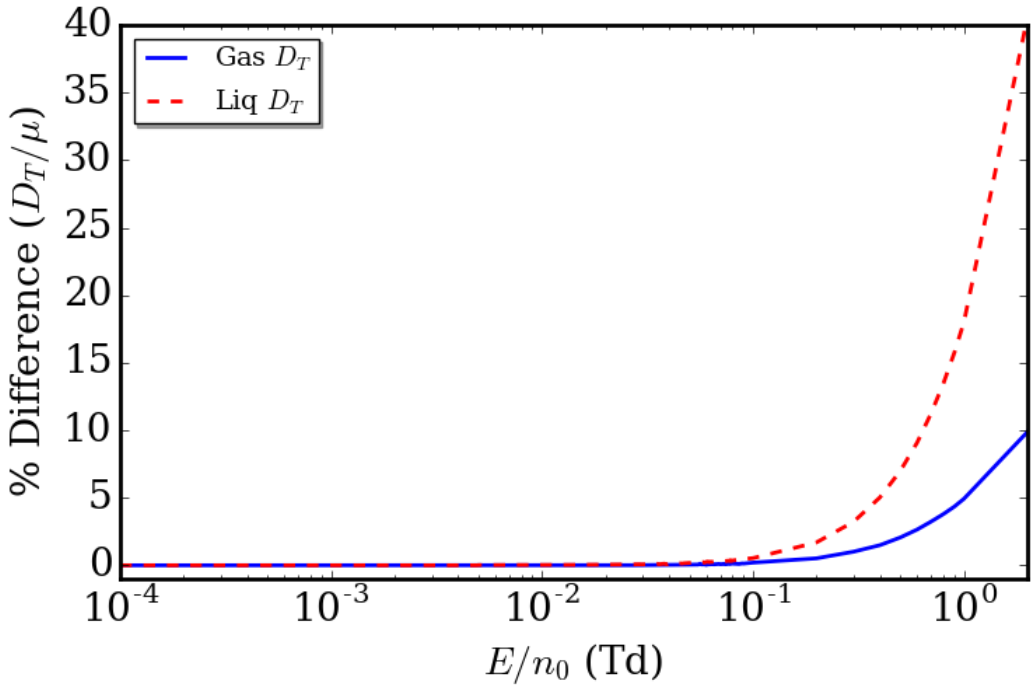

Figure 7. Percentage differences between the two-term and multi-term values of the characteristic energy for the gas (Gas) and liquid (Liq) phases. All percentages are relative to the converged multi-term result using the full differential cross-section.

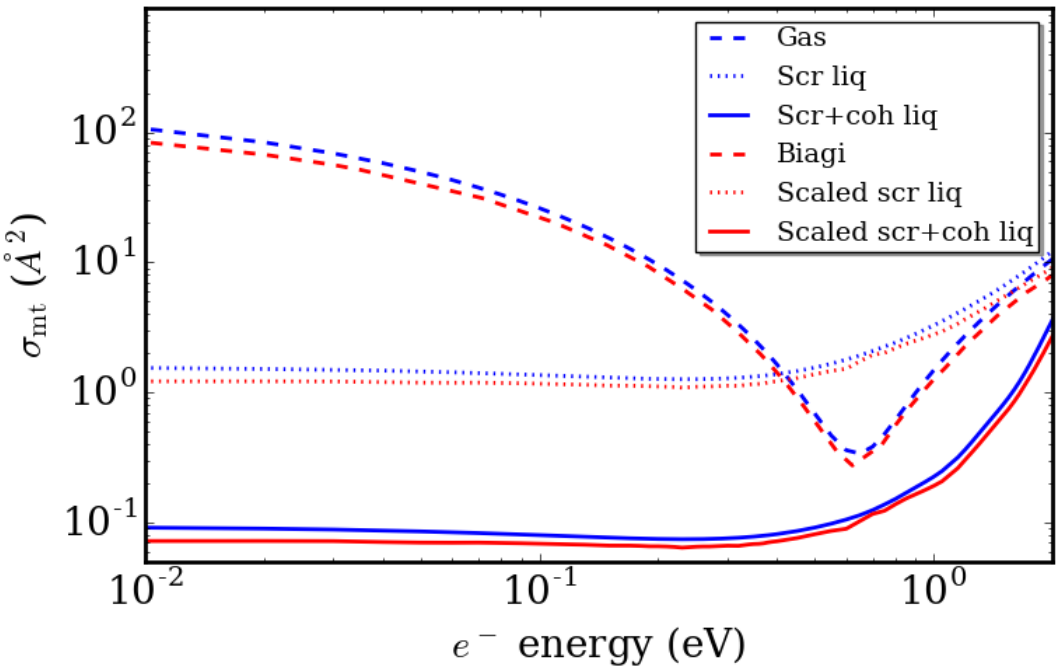

Figure 8. The momentum transfer cross-sections in the gas-phase (Gas; Biagi), liquid-phase (Scr liq, Scaled scr liq) and including their modifications when coherent scattering effects are included (Scr+coh liq, Scaled scr+coh liq).

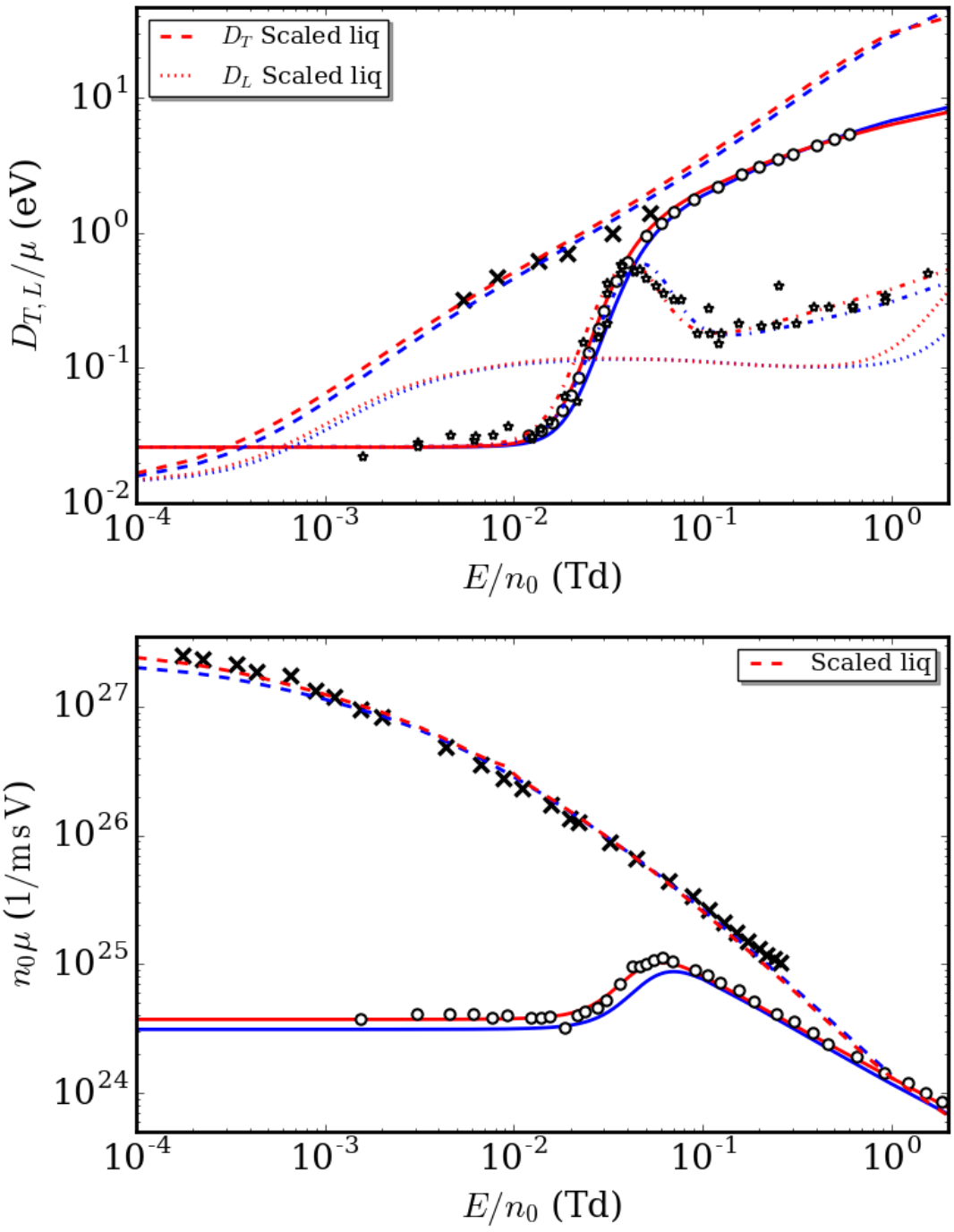

Figure 9. Comparison of the transverse (D_T/μ) and longitudinal (D_L/μ) characteristic energies (top) and reduced mobilities ($n_0\mu$) (bottom) in gaseous and liquid xenon, with those calculated from the various approximations to the cross-sections. The current liquid-phase cross-sections (Liq) have been calculated including coherent scattering effects. All other profiles are the same as in Figure 5. The calculations using the re-scaled Biagi cross-sections are given by the red lines (Scaled liq). All other profiles are the same as given in Figures 5 and 6.